

# A kinetic investigation of unimolecular reactions involving trace metals at post-combustion flue gas conditions

Jennifer Wilcox

Department of Energy Resources Engineering, School of Earth Sciences, Stanford University,  
Green Earth Sciences 065, 367 Panama Street, Stanford, CA 94305, USA.  
Email: wilcoxj@stanford.edu

**Environmental context.** Understanding trace metal speciation in coal combustion flue gases is imperative to the design of effective capture technologies to prevent their release into the atmosphere. Unfortunately much of the kinetics that dictate trace metal speciation are not known and the current study focuses for the first time on the kinetics for three reactions involving mercury and one involving selenium. Rate constant expressions are provided over a broad temperature range (i.e. 298–2000 K), indicative of post-combustion flue gas conditions.

**Abstract.** Ab-initio methods were carried out to calculate forward and reverse rate constant data for the following reactions:  $\text{Hg} + \text{Cl}_2 \leftrightarrow \text{HgCl}_2$ ,  $\text{HgCl} + \text{Cl} \leftrightarrow \text{HgCl}_2$ ,  $\text{Hg} + \text{O} \leftrightarrow \text{HgO}$ , and  $\text{Se} + \text{H}_2 \leftrightarrow \text{SeH}_2$ . Theoretical predictions of bond distances, vibrational frequencies and enthalpies of reaction are compared to available experimental data to determine the level of theory most appropriate for predicting kinetic parameters. The pseudopotentials ECP60MDF and RECP60VDZ were used for mercury in combination with B3LYP or QCISD(T) methods whereas the complete 6–311++G(3df,3pd) Pople basis set with the CCSD(T) method was used for selenium. Potential energy curves for each reaction were constructed and a variational approach along with RRKM theory was used to predict rate constants from 298 to 2000 K. Reactions  $\text{HgCl} + \text{Cl} \leftrightarrow \text{HgCl}_2$  and  $\text{Hg} + \text{O} \leftrightarrow \text{HgO}$  were found to have a strong negative temperature dependence, whereas the insertion reactions  $\text{Hg} + \text{Cl}_2 \leftrightarrow \text{HgCl}_2$  and  $\text{Se} + \text{H}_2 \leftrightarrow \text{SeH}_2$  were found to proceed very slowly with large pre-exponential factors.

## Introduction

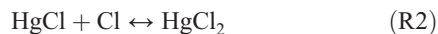
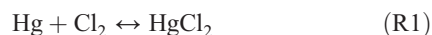
The combustion of coal continues to be a substantial source of energy in the United States; approximately half of the electricity generated is derived from coal according to the Department of Energy (Energy Information Administration, see <http://www.eia.doe.gov/neic/infosheets/electricgeneration.html>, accessed January 2011). The harmful emissions of trace metals created during the combustion process<sup>[1–3]</sup> have garnered much attention in the past decade with various state-wide environmental regulations being enacted to limit their release into the atmosphere. As a result, there is a much greater need for effective removal strategies of trace metals such as mercury and selenium and, correspondingly, much more interest in work regarding their reaction kinetics and related speciation.<sup>[4–6]</sup>

The primary source of domestic anthropogenic Hg emissions is through the combustion of coal in power plants, and on 15 March 2005 the USA EPA issued the Clean Air Mercury Rule to reduce Hg emissions from coal-fired power plants by 69% from 1999 levels by the year 2018.<sup>[7]</sup> A February 2008 decision by the US District of Columbia Circuit Court of Appeals remanded the Clean Air Mercury Rule back to the US Environmental Protection Agency (for additional information please refer to the document vacating EPA's rule by the Washington, DC, circuit court thereby removing power plants from the Clean Air Act list of sources of hazardous air pollutants, see <http://www.epa.gov/camr/>, accessed January 2011), opening the possibility of more stringent federal emission limits similar to those already adopted by some states. To meet these limits, high mercury removals based on Maximum Achievable

Control Technology (MACT) for individual power plants may be needed. It is anticipated that MACT will include Hg in addition to other trace metals such as selenium (Se) (for additional information please check Clean Air Act (Section 112) at <http://www.epa.gov/camr/>, accessed January 2011). The likely predominant forms of mercury are elemental ( $\text{Hg}^0$ ) and oxidised ( $\text{HgCl}_2$ ), the former being the chief constituent at high temperatures (above 850 K) and the latter being the principal Hg species at lower temperatures (below 800 K), but highly dependent upon the chlorine content of the coal.<sup>[8]</sup> From thermochemical equilibrium calculations, mercuric oxide ( $\text{HgO}$ ) may also exist at approximately the same temperature as the  $\text{Hg}/\text{HgCl}_2$  crossover, i.e.  $\sim 825$  K, and may continue to exist in small quantities at higher temperatures.<sup>[9]</sup> Because  $\text{HgCl}_2$  is soluble in water, its removal is ideal through the use of wet scrubbers originally in place for  $\text{SO}_2$  removal; therefore, knowledge of possible mechanisms for  $\text{HgCl}_2$  formation may allow for modifications in combustion conditions to enhance  $\text{Hg}^0$  conversion to this oxidised form. The aim of the current work is to add mercury oxidation reaction pathway kinetics to the existing body of knowledge for implementation into global combustion models.<sup>[10–13]</sup>

Selenium speciation in flue gas has also been investigated<sup>[14,15]</sup> and although very little kinetic data are available for Se reactions, a previous thermodynamic study<sup>[16]</sup> shows that  $\text{SeH}_2$  is the predominant Se species under reducing conditions, which would be applicable to coal gasification applications. Previous investigations have focussed on the reaction pathways involving  $\text{SeO}_2$ , which is thought to be the prevalent species under

oxidising conditions.<sup>[16–18]</sup> The current work is the first to investigate the direct H<sub>2</sub> insertion reaction to the formation of SeH<sub>2</sub>.



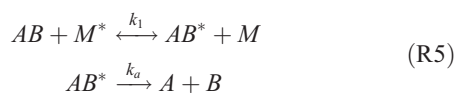
Rate constants are obtained in this work for reactions 1 through 4 by variationally minimising the universal Rice–Ramsperger–Kassel–Marcus (RRKM) rate constant with respect to the position of the generalised transition state along the reaction coordinate, similar to previous work.<sup>[19]</sup>

### Computational methodology

Calculations were carried out using the Gaussian 03 suite of programs.<sup>[20]</sup> Basis sets incorporating relativistic effects were employed through the use of small-core relativistic effective core potentials (RECP) for the inner electrons of mercury. A relativistic compact effective potential, RECP60VDZ of the Stevens group,<sup>[21]</sup> which replaces 60 of mercury's atomic core electrons, derived from numerical Dirac–Fock wave functions using an optimising process based upon the energy-overlap functional was used. Energy-optimised (5s5p)/[2s2p] Gaussian-type double- $\zeta$  quality sp and triple- $\zeta$  quality d functions were used, with the triple- $\zeta$  d functions essential for describing the orbital shape changes that exist with d occupancy. The second basis set carried out for mercury relies upon the relativistic ECP60MDF pseudopotential of the Stuttgart group<sup>[22]</sup> with the energy-optimised (8s8p7d)/[6s6p4d] Gaussian-Type Orbital (GTO) valence basis optimised using multiconfiguration Dirac–Fock (MCDF) calculations. For selenium and other species such as chlorine, oxygen and hydrogen, a complete Pople<sup>[23]</sup> basis set that incorporates both diffuse and polarisation functions was employed, i.e. 6–311++G(3df,3pd). The optimal basis set and method combination were chosen based upon a comparison of bond distances, vibrational frequencies and theoretical reaction enthalpy predictions to experiment.

### Kinetic calculations

To determine the unimolecular decomposition rate constants for the reverse of reactions 1–4, RRKM theory was carried out using the Holbrook et al.<sup>[24]</sup> test on Unimolecular Reactions as a guide. For the forward reactions, the experimental equilibrium constants along with the RRKM-derived unimolecular rate constant data were used. RRKM theory models a unimolecular decomposition reaction as a two-step process following the general form shown in reaction 5 where  $AB$  is the reactant molecule,  $M$  is the collision partner, and \* indicates that the species is energised:



The overall rate constant expression ( $k_{uni}$ ) is given in Eqn 1, in which the rate constants of both the deactivation (reverse of first

step of reaction 5) and the decomposition (second step of reaction 5) are taken into account:

$$k_{uni} = \frac{LQ_1^+}{N_a h Q_1 Q_2} e^{\left[\frac{-E_0}{RT}\right]} \Delta E \cdot \sum (X) \quad (1)$$

In Eqn 1, the statistical factor ( $L$ ) is the number of possible ways the reaction can proceed to obtain a desired product. For instance in the case of HgCl decomposition,  $L = 1$  as there is only one way in which the species can dissociate into Hg and Cl atoms. The quantity  $Q_1^+$  is the rotational partition function of the adiabatic rotations of the activated complex,  $Q_1$  is the rotational partition function of the reactant, and  $Q_2$  is the vibrational partition function of the reactant. Additionally, the activation energy ( $E_0$ ) is the difference between the reactant energy and the minimum needed to cross the barrier, whereas  $E^*$  is the energy of each state relative to  $E_0$ , and  $\Delta E$  is the step size between states. The sum over states ( $X$ ) is defined as:

$$X = \frac{W}{1 + \frac{k_a}{\beta_c Z_{LJ}[M]}} e^{\left[\frac{-(E^* - E_0)}{RT}\right]} \quad (2)$$

such that

$$k_a = \frac{L Q_1^+ W}{N_a h Q_1 \rho} \quad (3)$$

The deactivation rate constant is represented by the  $\beta_c Z_{LJ}[M]$  term whereas the decomposition rate constant ( $k_a$ ) is given by Eqn 3. The collisional efficiency factor ( $\beta_c$ ) was selected as a value of 0.1, as the reactions were assumed to be in an inert bath gas,<sup>[25]</sup> and  $[M]$  is simply the concentration of the collision partner. The equation for the Lennard–Jones parameter (Eqn 2) is as follows:

$$Z_{LJ} = N_a \sigma_{am}^2 \sqrt{\frac{8RT}{\pi \mu_{am}}} \Omega_{am} \quad (4)$$

such that

$$\Omega_{am} = \left[ 0.636 + 0.567 \log\left(\frac{kT}{\epsilon_{am}}\right) \right]^{-1} \quad \text{when } 0.3 \leq \frac{kT}{\epsilon_{am}} \leq 500 \quad (5)$$

$$\Omega_{am} = \left[ 0.697 + 0.5185 \log\left(\frac{kT}{\epsilon_{am}}\right) \right]^{-1} \quad \text{when } 3 \leq \frac{kT}{\epsilon_{am}} \leq 300 \quad (6)$$

and

$$\frac{\epsilon_{am}}{k} = 65.3 T_c Z_c^{18} \quad (7)$$

Within Eqn 4,  $\mu$  represents the reduced mass and  $\sigma$  the collision diameter, in which the subscript ‘am’ refers to the reactant molecule ( $A$ ) and the collision partner ( $M$ ). In determining the Lennard–Jones parameter, a correction factor ( $\Omega$ ) is also used and is calculated using either Eqn 5 or 6. The value of  $\epsilon_{am}/k$  is found using Eqn 7 using critical temperature and compressibility data.

The energy level consists of a series of steps above that of the transition structure, as predicted by the Lindemann–Hinshelwood mechanism; the number of steps for any given reaction will depend upon the step size ( $\Delta E$ ) and the maximum energy ( $E_{\max}$ ). These are both selected arbitrarily but  $\Delta E$  is typically between 0.4 and 2.0 kJ mol<sup>-1</sup> [24] (30–170 cm<sup>-1</sup>), whereas  $E_{\max}$  has been chosen to be a value of 9000 cm<sup>-1</sup>.

Once the values of  $\Delta E$  and  $E_{\max}$  are determined, the sum and density of states are calculated at each energy level using the Beyer–Swinehart algorithm. [26] This algorithm predicts how many linear combinations of the vibrational frequencies, i.e. states that exist between  $E_0$  and  $E_{\max}$ , and determines which energy level they exist at based upon their magnitude. Each energy range will then have several states associated within it; the density of states ( $\rho$ ) for each range is the number of states divided by the step size ( $\Delta E$ ), whereas the sum of states ( $W$ ) is a direct count of how many states exist at or below the current energy level. By finding  $W$  and  $\rho$  at each energy level, the value of  $k_a$  at the corresponding levels can be determined and thus the overall sum of the quantity  $X$  used in calculating the rate constant ( $k_{uni}$ ).

## Results and discussion

### Vibrational frequency and bond distance comparison

The predicted vibrational frequencies of the ground states of HgCl, HgCl<sub>2</sub>, HgO and SeH<sub>2</sub> have been compared to available experimental data as shown in Table 1. There have been two reports of experimental vibrational frequencies for HgCl in the literature, i.e. 292.6 cm<sup>-1</sup> [27] and 298.97 cm<sup>-1</sup>. [28] At the B3LYP/ECP60MDF and B3LYP/RCEP60VDZ levels of theory, the predicted vibrational frequency is 260 and 244 cm<sup>-1</sup> respectively. Both levels of theory predicted the HgCl<sub>2</sub> vibrational frequencies with higher accuracy. The doubly-degenerate  $\Pi_u$  state has a reported experimental vibrational frequency of 100 cm<sup>-1</sup>, [29] with the best prediction lying within 10 cm<sup>-1</sup> at

92 cm<sup>-1</sup> at the B3LYP/RCEP60VDZ level of theory. Experimentally, it has been difficult to measure the  $\Sigma_g$  state, with many reports available in the literature, ranging from 313 to 366 cm<sup>-1</sup>. [30,31] Both levels of theory investigated fall within this range, with predictions of 319 and 318 cm<sup>-1</sup> for B3LYP/ECP60MDF and B3LYP/RCEP60VDZ levels of theory respectively. Finally, the  $\Pi_u$  state has also been reported with measured values of 376 cm<sup>-1</sup> [31] and 413 cm<sup>-1</sup>, [32] with the best prediction lying within 2 cm<sup>-1</sup> at 374 cm<sup>-1</sup> at the B3LYP/RCEP60VDZ level of theory. The following vibrational frequencies of SeH<sub>2</sub> have been measured by Hill and Edwards [33] and compare reasonably well with theoretical predictions in parentheses at the CCSD(T)/6-311++G(3df,3pd) level of theory: 2453.77 cm<sup>-1</sup> (2471), 2438.66 cm<sup>-1</sup> (2460) and 1053.16 cm<sup>-1</sup> (1061). To the author's knowledge there exists no vibrational frequency measurements for in the literature.

Table 1 also includes a comparison of the predicted equilibrium bond distances to available measured data. Experimental measurements [34–36] of HgCl bond distances range from 2.36 to 2.50 Å. Both levels of theory investigated predict bond distances within this range. The experimental bond distances [32,34,37] for HgCl<sub>2</sub> range from 2.25 to 2.44 Å. Again, both levels of theory fall within this range with predictions of 2.32 and 2.31 Å at the B3LYP/ECP60MDF and B3LYP/RCEP60VDZ levels of theory respectively. The QCISD(T)/RCEP60VDZ level of theory predicts a bond distance of 2.07 Å for HgO, which agrees reasonably well with the experimental value [38] of 2.03 Å from X-ray diffraction measurements. The CCSD(T)/6-311++G(3df,3pd) level of theory predicts an angle of 90.43° and an equilibrium bond distance of 1.420 Å, which compare reasonably well to the experimental measurements of Hill, [33] i.e. an angle of 90.34° with a bond distance of 1.460 Å.

### Reaction enthalpy comparison

In addition to the geometry and vibrational frequency predictions, the thermochemistry of reactions 1 and 4 have also been

**Table 1.** Comparison between experimental and theoretical vibrational frequencies and bond distances

	Experiment	B3LYP/ECP60MDF	B3LYP/RCEP60VDZ
Vibrational frequency comparison (cm <sup>-1</sup> )			
HgCl	292.6, <sup>[27]</sup> 298.97 <sup>[28]</sup>	260	244
HgCl <sub>2</sub> (symmetric stretch)	376, <sup>[31]</sup> 413 <sup>[32]</sup>	373	374
(asymmetric stretch)	313–366 <sup>[30]</sup>	319	318
(bend)	100 <sup>[29]</sup>	84, 84	92, 92
		QCISD(T)/RCEP60VDZ	
HgO	NA		390
		CCSD(T)/6-311++G(3df,3pd)	
SeH <sub>2</sub> (symmetric stretch)	2453.77 <sup>[33]</sup>		2471
(asymmetric stretch)	2438.66 <sup>[33]</sup>		2460
(scissors)	1053.16 <sup>[33]</sup>		1061
Bond distance comparison (Å)			
HgCl	2.36–2.50 <sup>[34–36]</sup>	2.4648	2.4896
HgCl <sub>2</sub>	2.25–2.44 <sup>[32,34,37]</sup>	2.3211	2.3195
		QCISD(T)/RCEP60VDZ	
HgO	2.03 <sup>[38]</sup>		2.0791
		CCSD(T)/6-311++G(3df,3pd)	
SeH <sub>2</sub>	∠ 90.34°; 1.460 <sup>[33]</sup>		∠ 90.43°; 1.4255

**Table 2.** Comparison between experimental and theoretical reaction enthalpies (kcal mol<sup>-1</sup>)

Reaction	Experiment	B3LYP/ECP60MDF	B3LYP/RCEP60VDZ
Hg + Cl <sub>2</sub> ↔ HgCl <sub>2</sub>	-51.634 <sup>[32]</sup>	-55.033	-41.369
HgCl + Cl ↔ HgCl <sub>2</sub>	-82.705 <sup>[32]</sup>	-79.445	-73.167
		QCISD(T)/RCEP60VDZ	
Hg + O ↔ HgO	-4.00, <sup>[42]</sup> -8.92, <sup>[39]</sup> -13.97, <sup>[40]</sup> -64.22 <sup>[32]</sup>		-10.58
		CCSD(T)/6-311++G(3df,3pd)	
Se + H <sub>2</sub> ↔ SeH <sub>2</sub>	-49.89 ± 0.14 <sup>[43]</sup>		-49.94

**Table 3.** Transition structure parameters

	HgCl <sub>2</sub> → Hg + Cl <sub>2</sub>	HgCl <sub>2</sub> → HgCl + Cl	HgO → Hg + O	SeH <sub>2</sub> → Se + H <sub>2</sub>
Bond length 1 (Å)	2.77	2.35	3.00	2.15
Bond length 2 (Å)	2.74	4.20	-	2.15
Bond angle (°)	57.2	180.0	-	25.0
Vibrational frequencies (cm <sup>-1</sup> )	105.31	27.12	-	1224.16
	222.08	27.12	-	2160.95
	-	320.18	-	-
	247.44i	91.3165i	95.42i	881.31i

examined and are compared to the experimental data<sup>[32]</sup> in Table 2. The experimental value reported for reaction 1 is -51.634 kcal mol<sup>-1</sup>. The theoretical prediction at the B3LYP/ECP60MDF level of theory underpredicts this value by just over 3 kcal mol<sup>-1</sup> at -55.033 kcal mol<sup>-1</sup>. The same level of theory also deviates from experiment for reaction 2 by ~3 kcal mol<sup>-1</sup>. Both HgCl<sub>2</sub> formation pathways are exothermic. The formation pathways of HgO and SeH<sub>2</sub> in reactions 3 and 4 respectively are also exothermic. To predict the experimental reaction enthalpy of reaction 3, the experimental enthalpy of formation of HgO must be known. This has received a great deal of attention in the literature with the reported experimental HgO enthalpy of formation in question. Many researchers have carried out high-level quantum-based simulations on the formation enthalpy of HgO and have predicted it to primarily range between 60.25 and 81.2 kcal mol<sup>-1</sup>.<sup>[39-42]</sup> The experimental data suggests a heat of formation of 10 kcal mol<sup>-1</sup>.<sup>[32]</sup> The enthalpies of reaction estimated from various sources of the HgO formation enthalpy are listed in Table 2 and range between -4.00 and -13.97 kcal mol<sup>-1</sup> from the theoretical predictions available in the literature, compared to an experimental-based<sup>[32]</sup> calculation of -64.22 kcal mol<sup>-1</sup>. At the QCISD(T)/RCEP60VDZ level of theory carried out in the current work an estimate of -10.58 kcal mol<sup>-1</sup> is predicted, which lies within the range of the previous theory-based predictions. Experimental data exists for reaction 4. Gibson et al.<sup>[43]</sup> carried out a photoionisation study on SeH<sub>2</sub> and predicted an enthalpy of reaction of -49.89 ± 0.14 kcal mol<sup>-1</sup>. At the CCSD(T)/6-311++G(3df,3pd) level of theory, a prediction of -49.94 kcal mol<sup>-1</sup> fits within this range.

#### Rate constant predictions

To the author's knowledge, no experimental rate constant data exist for any of the four reactions investigated. For each reaction, potential energy curves have been generated at the level of theory that most accurately predicts the experimental vibrational frequency, bond distance and reaction enthalpy. Saddle points have been identified by having one imaginary frequency.

Table 3 lists the geometric and vibrational frequency data for the transition structures identified for each reaction. Reactions 1 and 4 are direct insertion reactions in which Hg and Se are directly inserted into the structure of Cl<sub>2</sub> and H<sub>2</sub> from the product species HgCl<sub>2</sub> and SeH<sub>2</sub> respectively. For reaction 1, the bond angle of the transition state is 57.2°, whereas the bond angle for reactions 4 is tighter at 25.0°. Reaction 2 was assumed to proceed via a linear transition structure. Table 4 lists the kinetic data required for the calculation of forward and reverse rate constants for reactions 1 and 4. The kinetics of each reaction were determined at the following levels of theory: B3LYP/ECP60MDF (Hg + Cl<sub>2</sub> ↔ HgCl<sub>2</sub> and HgCl + Cl ↔ HgCl<sub>2</sub> reactions), QCISD(T)/RCEP60VDZ (Hg + O ↔ HgO), and CCSD(T)/6-311++G(3df,3pd) (Se + H<sub>2</sub> ↔ SeH<sub>2</sub>). The forward rate constants of reactions 1 and 4 were calculated from the product of the equilibrium constant ( $K_{eq}$ ) obtained from experiment<sup>[32]</sup> and the RRKM-derived reverse rate constant for the unimolecular decomposition. The two direct insertion reactions involving HgCl<sub>2</sub> and SeH<sub>2</sub> proceeded in an Arrhenius fashion with fairly small preexponential factors for the forward recombination directions, e.g.  $1.77 \times 10^5$  cm<sup>3</sup> mol<sup>-1</sup> s<sup>-1</sup> for HgCl<sub>2</sub> and  $1.36 \times 10^{10}$  cm<sup>3</sup> mol<sup>-1</sup> s<sup>-1</sup> for the SeH<sub>2</sub> formation pathways. For the reverse reactions, the dissociation barriers required for the trigonal planar configuration were quite high at 85.75 kcal mol<sup>-1</sup> for HgCl<sub>2</sub> ↔ Hg + Cl<sub>2</sub> and 70.23 kcal mol<sup>-1</sup> for the SeH<sub>2</sub> ↔ Se + H<sub>2</sub> decomposition pathways. For the last two reactions investigated, the rate constants for the radical-radical recombination reaction, HgCl + Cl ↔ HgCl<sub>2</sub> and atom-radical recombination reaction, Hg + O ↔ HgO, were found to decrease as temperature increased. These rate constants could still be expressed in an Arrhenius fashion, but it would require a negative activation energy to capture the trend accurately. Both reactions are nearly barrierless in the forward direction. Increasing the temperature provides increased energy to an activated complex making it less likely for the complex to proceed to the potential well through the product channel. The rate expressions for these reactions are represented by a power law expression, e.g.  $k = A \times (T/298)^n$ , as shown in Table 4.



**Table 4. Kinetic and thermodynamic parameters for forward and reverse reactions**  
 $K_{\text{eq}}$  data taken from Chase et al.<sup>[32]</sup>

Reaction	Forward		Reverse		$K_{\text{eq}}$
	$E_a$ (kcal mol <sup>-1</sup> )	$A$ (cm <sup>3</sup> mol <sup>-1</sup> s <sup>-1</sup> )	$E_a$ (kcal mol <sup>-1</sup> )	$A$ (s <sup>-1</sup> )	
Hg + Cl <sub>2</sub> ↔ HgCl <sub>2</sub> B3LYP/ECP60MDF	8.64	1.77 × 10 <sup>5</sup>	85.75	1.8 × 10 <sup>6</sup>	2.99 × 10 <sup>32</sup>
Se + H <sub>2</sub> ↔ SeH <sub>2</sub> CCSD(T)/6-311++G(3df,3pd)	5.83	1.36 × 10 <sup>10</sup>	70.23	2.31 × 10 <sup>10</sup>	9.84 × 10 <sup>29</sup>
	Forward Form: $k = A \times (T/298)^n$		Reverse Form: $k = A \times e^{-E_a/RT}$		
	$n$	$A$ (cm <sup>3</sup> mol <sup>-1</sup> s <sup>-1</sup> )	$E_a$ (kcal mol <sup>-1</sup> )	$A$ (s <sup>-1</sup> )	
HgCl + Cl ↔ HgCl <sub>2</sub> B3LYP/ECP60MDF	-8.567	7.00 × 10 <sup>11</sup>	76.08	1.35 × 10 <sup>8</sup>	2.06 × 10 <sup>55</sup>
Hg + O ↔ HgO QCISD(T)/RCEP60VDZ	-3.037	5.62 × 10 <sup>5</sup>	7.51	1.75 × 10 <sup>4</sup>	4.88 × 10 <sup>2</sup> <sup>A</sup>

<sup>A</sup>Based upon theoretical predictions of HgO enthalpy of formation.

The dissociation pathway of HgCl<sub>2</sub> (reverse reaction) proceeds with a significant barrier of 79.32 kcal mol<sup>-1</sup>, whereas the dissociation of HgO is substantially smaller at 7.51 kcal mol<sup>-1</sup>.

Although an accurate analysis of this data requires their input into a global model, some general conclusions can be made regarding the relative thermodynamic stability and relative time scales associated with each of the four reactions investigated. For instance, investigation of the forward kinetics at ambient conditions, reveals that reaction 3 is the most kinetically-favoured reaction, whereas the direct oxidation of Hg via Cl<sub>2</sub> in reaction 1 is the slowest of the reactions, which is not surprising given its low pre-exponential factor. At higher temperatures (e.g. 2000 K, indicative of exit boiler conditions) reaction 1 becomes competitive with reactions 3 and 4 as these are both kinetically-limited as temperature increases. In terms of thermodynamic stability, the product channel of reaction 3 is favoured to a much greater extent than the product channel of reaction 1. In total, these data are intended for use over a broad temperature range spanning the conditions of post-combustion flue gases in order to more accurately determine trace metal speciation, which will aid in the design of more effective control technologies for these volatile and environmentally harmful compounds.

### Acknowledgements

This material is based upon work partially supported by the National Science Foundation (NSF), Combustion and Plasma Division under Grant No. 0448758. The computational resources were supported by NSF through TeraGrid resources provided by TACC.

### References

- [1] M. H. Keating, *Mercury study report to congress. Volume II: Inventory of anthropogenic mercury emissions in the United States 1997* (US Environmental Protection Agency, Office of Air Quality Planning and Standards).
- [2] F. Slemr, G. Schuster, W. Seiler, Distribution, speciation, and budget of atmospheric mercury. *J. Atmos. Chem.* **1985**, *3*, 407. doi:10.1007/BF00053870
- [3] A. W. Andren, D. H. Klein, Selenium in coal-fired steam plant emissions. *Environ. Sci. Technol.* **1975**, *9*, 856. doi:10.1021/ES60107A002
- [4] M. Diaz-Somoano, M. R. Martinez-Tarazona, Retention of arsenic and selenium compounds using limestone in a coal gasification flue gas. *Environ. Sci. Technol.* **2004**, *38*, 899. doi:10.1021/ES034344B
- [5] R. Agnihotri, S. Chauk, S. Mahuli, L.-S. Fan, Selenium removal using Ca-based sorbents: reaction kinetics. *Environ. Sci. Technol.* **1998**, *32*, 1841. doi:10.1021/ES971119J
- [6] N. C. Widmer, J. A. Cole, W. R. Seeker, J. A. Gaspar, Practical limitation of mercury speciation in simulated municipal waste incinerator flue gas. *Combust. Sci. Tech.* **1998**, *134*, 315. doi:10.1080/00102209808924138
- [7] S. E. Olson, C. R. Crocker, S. E. Benson, J. H. Pavlish, M. J. Holmes, Surface compositions of carbon sorbents exposed to simulated low-rank coal flue gases. *J. Air Waste Manage. Assoc.* **2005**, *55*, 747.
- [8] R. N. Sliker, J. C. Kramlich, N. M. Marinov, Towards the development of a chemical kinetic model for the homogeneous oxidation of mercury by chlorine species. *Fuel Process. Technol.* **2000**, *65*–*66*, 423. doi:10.1016/S0378-3820(99)00108-3
- [9] C. L. Senior, A. F. Sarofim, T. Zeng, J. J. Helble, R. Mamani-Paco, Gas-phase transformations of mercury in coal-fired power plants. *Fuel Process. Technol.* **2000**, *63*, 197. doi:10.1016/S0378-3820(99)00097-1
- [10] J. Wilcox, J. Robles, D. C. J. Marsden, P. Blowers, Theoretically predicted rate constants for mercury oxidation by hydrogen chloride in coal combustion flue gases. *Environ. Sci. Technol.* **2003**, *37*, 4199. doi:10.1021/ES034025K
- [11] J. Wilcox, D. C. J. Marsden, P. Blowers, Evaluation of basis sets and theoretical methods for estimating rate constants of mercury oxidation reactions involving chlorine. *Fuel Process. Technol.* **2004**, *85*, 391. doi:10.1016/J.FUPROC.2003.09.007
- [12] J. Wilcox, A Kinetic Investigation of high-temperature mercury oxidation by chlorine. *J. Phys. Chem. A* **2009**, *113*, 6633. doi:10.1021/JP901050D
- [13] B. Krishnakumar, J. J. Helble, Understanding mercury transformations in coal-fired power plants: evaluation of homogeneous Hg oxidation mechanisms. *Environ. Sci. Technol.* **2007**, *41*, 7870. doi:10.1021/ES071087S
- [14] R. Yan, D. Gauthier, G. Flamant, Possible interactions between As, Se, and Hg during coal combustion. *Combust. Flame* **2000**, *120*, 49. doi:10.1016/S0010-2180(99)00079-6

- [15] M. P. Pavageau, A. Morin, F. Seby, C. Guimon, E. Krupp, C. Pecheyran, J. Poulleau, O. F. X. Donard, Partitioning of metal species during an enriched fuel combustion experiment. Speciation in the gaseous and particulate phases. *Environ. Sci. Technol.* **2004**, *38*, 2252. doi:10.1021/ES034408I
- [16] R. Yan, D. Gauthier, G. Flamant, G. Peraudeau, Fate of selenium in coal combustion: volatilization and speciation in the flue gas. *Environ. Sci. Technol.* **2001**, *35*, 1406. doi:10.1021/ES00011005
- [17] D. Urban, J. Wilcox, A theoretical study of properties and reactions involving arsenic and selenium compounds present in coal combustion flue gases. *J. Phys. Chem. A* **2006**, *110*, 5847. doi:10.1021/JP055564+
- [18] M. T. Monahan-Pendergast, M. Przybylek, M. Lindblad, J. Wilcox, Theoretical predictions of arsenic and selenium species under atmospheric conditions. *Atmos. Environ.* **2008**, *42*, 2349. doi:10.1016/J.ATMOSENV.2007.12.028
- [19] J. Wilcox, P. Blowers, Decomposition of mercuric chloride and application to combustion flue gases. *Environ. Chem.* **2004**, *1*, 166. doi:10.1071/EN04036
- [20] M. J. Frisch, G. W. Trucks, H. B. Schlegel, G. E. Scuseria, M. A. Robb, J. R. Cheeseman, J. A. Montgomery, Jr, T. Vreven, K. N. Kudin, J. C. Burant, J. M. Millam, S. S. Iyengar, J. Tomasi, V. Barone, B. Mennucci, M. Cossi, G. Scalmani, N. Rega, G. A. Petersson, H. Nakatsuji, M. Hada, M. Ehara, K. Toyota, R. Fukuda, J. Hasegawa, M. Ishida, T. Nakajima, Y. Honda, O. Kitao, H. Nakai, M. Klene, X. Li, J. E. Knox, H. P. Hratchian, J. B. Cross, V. Bakken, C. Adamo, J. Jaramillo, R. Gomperts, R. E. Stratmann, O. Yazyev, A. J. Austin, R. Cammi, C. Pomelli, J. W. Ochterski, P. Y. Ayala, K. Morokuma, G. A. Voth, P. Salvador, J. J. Dannenberg, V. G. Zakrzewski, S. Dapprich, A. D. Daniels, M. C. Strain, O. Farkas, D. K. Malick, A. D. Rabuck, K. Raghavachari, J. B. Foresman, J. V. Ortiz, Q. Cui, A. G. Baboul, S. Clifford, J. Cioslowski, B. B. Stefanov, G. Liu, A. Liashenko, P. Piskorz, I. Komaromi, R. L. Martin, D. J. Fox, T. Keith, M. A. Al-Laham, C. Y. Peng, A. Nanayakkara, M. Challacombe, P. M. W. Gill, B. Johnson, W. Chen, M. W. Wong, C. Gonzalez, J. A. Pople, *Gaussian 03, Revision C.02* **2004** (Gaussian, Inc.: Wallingford, CT).
- [21] W. J. Stevens, M. Krauss, Relativistic compact effective core potentials and efficient, shared-exponent basis sets for the third-, fourth-, and fifth-row atoms. *Can. J. Chem.* **1992**, *70*, 612. doi:10.1139/V92-085
- [22] D. Figgen, G. Rauhut, M. Dolg, H. Stoll, Energy-consistent pseudopotentials for group 11 and 12 atoms: adjustment to multi-configuration Dirac–Hartree–Fock data. *Chem. Phys.* **2005**, *311*, 227. doi:10.1016/J.CHEMPHYS.2004.10.005
- [23] R. Krishnan, J. S. Binkley, R. Seeger, J. A. Pople, Self-consistent molecular orbital methods. XX. A basis set for correlated wave functions. *J. Chem. Phys.* **1980**, *72*, 650. doi:10.1063/1.438955
- [24] K. A. Holbrook, M. J. Pilling, S. H. Robertson, *Unimolecular Reactions*, 2nd edn **1996** (Wiley: Chichester, UK).
- [25] K. J. Laidler, *Chemical Kinetics*, 3rd edn **1987** (Harper and Row: New York).
- [26] T. Beyer, D. F. Swinehart, Algorithm 448. Number of multiple-restricted partitions. *Commun. ACM* **1973**, *16*, 379[A1]. doi:10.1145/362248.362275
- [27] J. Tellinghuisen, J. G. Ashmore, The B → X transition in <sup>200</sup>Hg<sup>79</sup>Br. *Appl. Phys. Lett.* **1982**, *40*, 867. doi:10.1063/1.92946
- [28] A. A. Malt'sev, G. K. Selivanov, V. I. Yampolsky, N. I. Zavalishin, Far infrared absorption spectra of mercury dihalide vapours. *Nat. Phys. Sci.* **1971**, *231*, 157.
- [29] B. J. Aylett, *Comprehensive Inorganic Chemistry* **1973** (Pergamon Press: New York).
- [30] S. Bell, R. D. McKenzie, J. B. Coon, The spectrum of HgCl<sub>2</sub> in the vacuum ultraviolet. *J. Mol. Spectrosc.* **1966**, *20*, 217. doi:10.1016/0022-2852(66)90023-3
- [31] D. M. Adams, D. J. Hill, Single-crystal infrared study and assignment for mercury(II) chloride and bromide. *J. Chem. Soc., Dalton Trans.* **1978**, 776. doi:10.1039/DT9780000776
- [32] M. W. Chase, Jr, C. A. Davies, J. R. Downey, D. J. Fruirip, R. A. McDonald, A. N. Syverud, JANAF thermochemical tables – 3rd edition. *J. Phys. Chem. Ref. Data* **1985**, *14*(Suppl. 2), 927.
- [33] R. A. Hill, T. H. Edwards, Vibrational analysis and isotope effects in hydrogen selenide. *J. Chem. Phys.* **1965**, *42*, 1391. doi:10.1063/1.1696127
- [34] M. Kaupp, H. G. von Schnering, Origin of the unique stability of condensed-phase Hg<sub>2</sub><sup>2+</sup>. An ab initio investigation of MI and MII species (M = Zn, Cd, Hg). *Inorg. Chem.* **1994**, *33*, 4179. doi:10.1021/IC00096A049
- [35] D. Strömberg, A. Strömberg, U. Wahlgren, Relativistic quantum calculations on some mercury sulfide molecules. *Water Air Soil Pollut.* **1991**, *56*, 681. doi:10.1007/BF00342309
- [36] T. R. Cundari, A. Yoshikawa, Computational study of methane activation by mercury(II) complexes. *J. Comput. Chem.* **1998**, *19*, 902. doi:10.1002/(SICI)1096-987X(199806)19:8<902::AID-JCC9>3.0.CO;2-T
- [37] D. Strömberg, O. Gropen, U. Wahlgren, Non-relativistic and relativistic calculations on some Zn, Cd, and Hg complexes. *Chem. Phys.* **1989**, *133*, 207. doi:10.1016/0301-0104(89)80202-2
- [38] S. Šćavničar, D. Grdenić, The crystal structure of oxy-mercuric-mercurous chloride. *Acta Crystallogr.* **1955**, *8*, 275. doi:10.1107/S0365110X55000881
- [39] M. J. S. Dewar, C. Jie, AM1 calculations for compounds containing mercury. *Organometallics* **1989**, *8*, 1547. doi:10.1021/OM00108A029
- [40] D. Strömberg, O. Gropen, U. Wahlgren, Non-relativistic and relativistic calculations on some zinc, cadmium, and mercury complexes. *Chem. Phys.* **1989**, *133*, 207. doi:10.1016/0301-0104(89)80202-2
- [41] J. A. Tossell, Calculation of the energetics for oxidation of gas-phase elemental Hg by Br and BrO. *J. Phys. Chem. A* **2003**, *107*, 7804. doi:10.1021/JP030390M
- [42] B. C. Shepler, K. A. Peterson, Mercury monoxide: a systematic investigation of its ground electronic state. *J. Phys. Chem. A* **2003**, *107*, 1783. doi:10.1021/JP027512F
- [43] S. T. Gibson, J. P. Greene, J. Berkowitz, A photoionization study of SeH and H<sub>2</sub>Se. *J. Chem. Phys.* **1986**, *85*, 4815. doi:10.1063/1.451715

Manuscript received 4 January 2011, accepted 3 March 2011